

# Long Term Variability of SDSS Quasars

W. H. de Vries, R. H. Becker

*University of California, One Shields Ave, Davis, CA 95616  
Lawrence Livermore National Laboratory, L-413, Livermore, CA 94550*

devries1@llnl.gov

and

R. L. White

*Space Telescope Science Institute, 3700 San Martin Drive, Baltimore, MD 21218*

## ABSTRACT

We use a sample of 3791 quasars from the Sloan Digital Sky Survey (SDSS) Early Data Release (EDR), and compare their photometry to historic plate material for the same set of quasars in order to study their variability properties. The time base-line we attain this way ranges from a few months to up to 50 years. In contrast to monitoring programs, where relatively few quasars are photometrically measured over shorter time periods, we utilize existing databases to extend this base-line as much as possible, at the cost of sampling per quasar. Our method, however, can easily be extended to much larger samples. We construct variability Structure Functions and compare these to the literature and model functions. From our modeling we conclude that 1) quasars are more variable toward shorter wavelengths, 2) their variability is consistent with an exponentially decaying light-curve with a typical time-scale of  $\sim 2$  years, 3) these outbursts occur on typical time-scales of  $\sim 200$  years. With the upcoming first data release of the SDSS, a much larger quasar sample can be used to put these conclusions on a more secure footing.

*Subject headings:* galaxies: active — galaxies: statistics — quasars: general

## 1. Introduction

It has been known for a long time that quasars are variable, both on short (days to weeks) and long (10's of years) timescales (e.g., Heckman 1976). There seems to be a consensus that the mechanisms causing these variations are distinct: the large amplitude short time-scale variations (mainly in BL Lac and OVV sources) are thought to be due to relativistic beaming effects (e.g., Bregman 1990, Fan & Lin 2000, Vagnetti et al. 2003), whereas the long-term small amplitude variations could possibly be due to accretion disk instabilities (e.g., Rees 1984, Siemiginowska & Elvis 1997, Kawaguchi et al. 1998), bursts of supernovae close to the nucleus (e.g., Terlevich et al. 1992, Cid Fernandes, Aretxaga, & Terlevich 1996), or even micro-lensing events by Galactic

compact objects (e.g., Hawkins 1993). Disentangling the various proposed models from observations has been particularly hard, partly because of the non-uniformity of the observations, samples, and applied methods in the literature (cf. Table 1 of Giveon et al. (1999) for a nice summary).

The classical approach tackling the variability problem is to monitor a relatively small sample of quasars (up to a few 100) over long periods of time, up to 20 years in cases. While this provides a well (time) sampled database of light-curves, it does so for a select set of objects. Given the wide range of correlations, anti-correlations, or the lack thereof, found for particular parameters across different data-sets and monitoring programs, sample selection is clearly an issue. In this Paper, therefore, we used the largest public quasar data-set

that has both multi-epoch optical photometry and redshift information. Only by enlarging the sample enough we feel that results are not going to be dominated by a few number of atypical objects.

We chose to use the Sloan Digital Sky Survey (SDSS) Early Data Release (EDR, Stoughton et al. 2002) quasar list, cross-correlated with the Second Generation Guide Star Catalog<sup>1</sup> (GSC2, McLean et al. 1998) and the Palomar Optical Sky Survey (POSS, Reid et al. 1991) imaging data. This resulted in a set of 3791 quasars, for which we have on average 7 epoch measurements over 2 passbands (cf. Sect. 2). While our approach does not provide very well sampled light-curves for individual quasars, or even accurate photometry, it does have a few distinct advantages. First of all, the sample is at least an order of magnitude larger than previous studies, minimizing the impact of peculiar sources. Secondly, all our sample quasars have redshift information, so we can correct for time-dilation effects. The time-baseline over which we have photometric data is  $\sim 50$  years, larger than previous work. But most importantly, the sample can be easily enlarged by significant factors, which has the potential to improve on the work presented here by quite a bit. The SDSS collaboration is preparing to make its first public data release soon.

The Paper is structured as follows: in Sect. 2 we present the careful calibration needed before one can use the variability data-set. Section 3 will discuss the results of our data analysis, its comparison to literature data and Monte Carlo modeling. The final Section (4) discusses the SDSS optical properties of the most variable subset of our sample.

## 2. Sample Selection and Calibration

Our sample is based on the SDSS EDR quasar list, which was cross-correlated with the GSC2 catalog. This resulted in a list of 3791 quasars (out of 3814 from the EDR list) with positional matches better than  $3''$ . The epoch base-line was extended by including POSS data from the 1950's. Not all of the 3791 quasars were retrieved from the older data, so for a subset of the quasars (1347

objects) the maximum base-line is limited to  $\sim 10$  years. Due to the spectroscopic requirements, our sample has an r-band limit of  $\sim 20.5$  magnitude (the mean is  $\bar{r} = 18.94$ ), considerably fainter than for instance work done on the Palomar Green (PG) quasars ( $B < 16$ , e.g., Giveon et al. 1999, Trevese & Vagnetti 2002). The quasar sample is drawn from a  $\sim 348$  square degree region of sky around zero declination (between  $-1.5^\circ$  and  $1.5^\circ$ ), and a small patch of  $\sim 33$  square degrees around  $17^{\text{h}}20^{\text{m}}$  and  $+60^\circ$  declination.

The data for the GSC2 was provided to us by the Space Telescope Science Institute, and the POSS data were taken from the USNO-A2 catalog server at Flagstaff. The more recent (and larger) USNO-B1 catalog (Monet et al. 2003) does not have a lot of 1950's era photometry, whereas USNO-A2 contains uniquely data from that epoch.

### 2.1. Passband Calibration

Given that none of the photometric data have been taken with the same telescope, detectors, and passbands, the relative calibration is particularly important. Even though both the photographic USNO-A2 and GSC2 catalogs have been calibrated with modern CCD measurements, various uncontrollables, like plate material sensitivity changes / degradation, render photographic plate calibration very difficult (see, for instance, Gal et al. 2003). Instead of relying on the cataloged magnitudes, we extracted all the stars within a 5 arcminute radius around each quasar position. These stars can then be used to calibrate and transform their magnitude (B and R for USNO-A2, and J and F for the GSC2 catalog) into the corresponding SDSS g and r-bands. The implicit assumption we make is that stars, on average, are not variable. With mean numbers of calibration stars per quasar of: 59 for USNO-A2, 47 for the GSC2, and 332 for the SDSS catalogs, we feel confident we are not affected by a small number of variable stars. All the extracted calibration stars were then position matched to within 3 arcseconds of each other to make sure the same stars are compared at the different epochs. This resulted in on average 36 position constant calibration stars per quasar (present in each epoch), for a total of  $\sim 0.5$  million calibration points. For each of the quasar fields, iterative least squares fits to the  $r_{sdss}$  to  $R_{usno-a2}$ ,  $r_{sdss}$  to  $F_{gsc2}$ ,  $g_{sdss}$  to  $B_{usno-a2}$ , and

<sup>1</sup>The Guide Star Catalogue-II is a joint project of the Space Telescope Science Institute and the Osservatorio Astronomico di Torino.

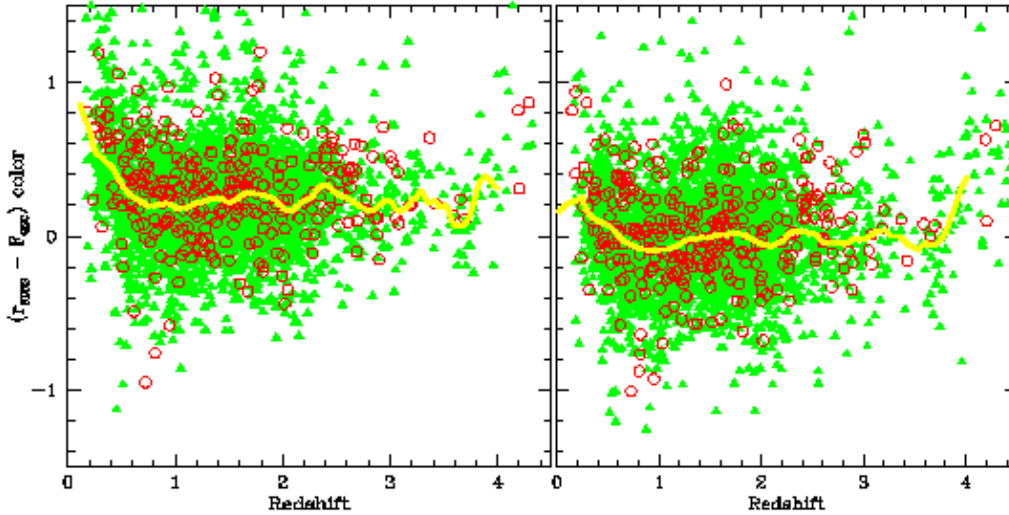


Fig. 1.— These two panels illustrate the importance of proper passband calibration. In the left panel, the uncorrected SDSS r-band to GSC2 F-band color is plotted as function of redshift. Note the offset toward positive r–F colors, mainly due to the fact that SDSS magnitudes are listed in the AB-mag system, and not in the Vega-mag system. After properly transforming F-band into r-band magnitudes using on average 36 stars per quasar, this residual color disappears for the most part (right panel). The radio-quiet quasars are solid green triangles, and the radio-loud quasars are open red circles, respectively. The yellow solid line is the median color as function of redshift. The upturn beyond  $z = 4$  is most likely due to absorption shortward of Ly- $\alpha$  entering the  $r_{sds}$ -band first.

$g_{sds}$  to  $J_{gsc2}$  color transformations were made, fitting both the (linear) slope and offset. To suppresses the impact of stellar variability (and measurement errors) even further,  $2\sigma$  outliers were excluded at each iteration.

The effectiveness of this calibration and passband transformation can be seen in Fig. 1, where the uncorrected  $(r_{sds} - F_{gsc2})$  color versus redshift distribution is plotted in the left panel. The thick solid line represents the sample median (per redshift bin), illustrating the redshift independent color offset for the quasars. This apparent offset vanishes after applying our stellar passband calibration (Fig. 1, right panel). All that remains are the “wiggles” due to various emission lines moving in and out of the passband (and which are very well modeled / removed by synthetic passbands and a quasar composite spectrum), and the apparent problem of measuring accurate magnitudes of extended sources on the POSS and GSC2 plates. The automated routines work well on point-sources, but they systematically overestimate resolved object magnitudes, resulting in

large, positive,  $(r_{sds} - F_{gsc2})$  values. This is illustrated by the upturn in the median curve toward low redshifts. With the decrease in optical size with increasing redshift, this effect becomes less important, and is essentially absent beyond  $z > 0.6$ .

While this calibration does take out plate-to-plate variations and gross color terms, it does *not* remove slight offsets due to the intrinsically different spectral shapes of quasars and stars. Fitting the best color transformation using the stars actually ensures that the color distribution (for the stars) has minimal scatter around a mean of zero, which is exactly the presumption we made. This minimization, while optimal for the stars, is not necessarily the best for the quasars. The  $B_{usno-a2}$  and  $J_{gsc2}$  filters<sup>2</sup> have bandpasses *bluer* than  $g_{sds}$ , whereas both the  $R_{usno-a2}$  and  $F_{gsc2}$  bands are *redder* than the corresponding  $r_{sds}$  (references for the photometric systems: Reid et al. (1991) for POSS and GSC2; and Stoughton et al. (2002) for

<sup>2</sup>effective photographic bandpasses, not physical filters

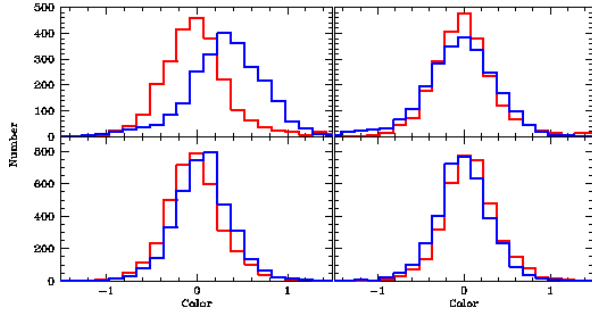


Fig. 2.— Color distributions before (left) and after the quasar–stellar spectral color correction. The top half of the plots concern the  $(g_{sdss} - B_{usno-a2})$  and  $(r_{sdss} - R_{usno-a2})$  colors (blue and red lines respectively), whereas the bottom parts are the  $(g_{sdss} - J_{gsc2})$ , and  $(r_{sdss} - F_{gsc2})$  colors (same coloring). The applied offsets, as determined by fitting Gaussian distributions to the histograms, are:  $+0.38$ ,  $-0.02$ ,  $+0.08$ , and  $-0.10$  (in the same color order).

the SDSS). Clearly, differences in spectral slopes for quasars and field stars will give rise to offsets in the color distributions, and of opposing signs between the blue and red bands.

This can be directly tested by plotting up the relevant histograms, as has been done in the left panel of Fig. 2. If we assume that the variations are random and distributed in a Gaussian fashion (the histograms in Fig. 2 are actually well fitted by Gaussians), we can measure the centroid offset accurately. The best fitting Gaussian functions, using a least squares (simulated annealing) minimization code, have means of:  $+0.38$ ,  $-0.02$ ,  $+0.08$ , and  $-0.10$ , for the color distributions  $(g_{sdss} - B_{usno-a2})$ ,  $(r_{sdss} - R_{usno-a2})$ ,  $(g_{sdss} - J_{gsc2})$ , and  $(r_{sdss} - F_{gsc2})$  respectively. The first indication that we are on the right track is that the offset *signs* behave in the expected way: the same on the blue (B and J to g) and red (R and F to r) side individually, and opposite across the blue and red side for each epoch. We can, however, do better. Assuming further that, since we are looking at mean properties, we can use mean quasar and stellar spectra (folded with the relevant passbands) to calculate what the offset values are supposed to be.

We present both the quasars composite spec-

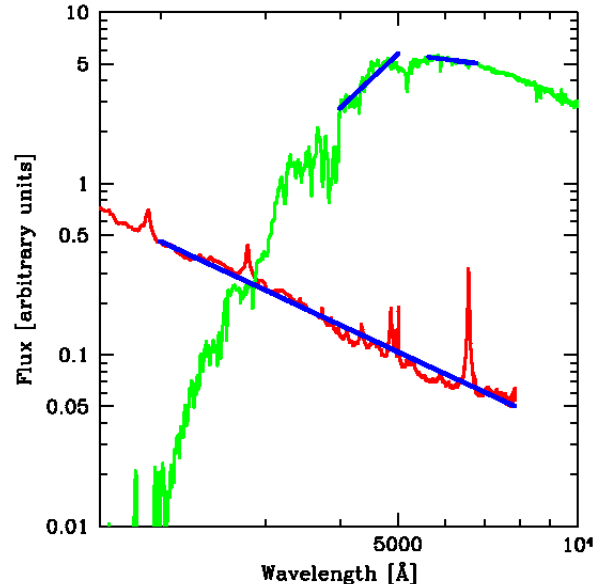


Fig. 3.— Composite spectra of our quasars (red curve), and K2 main sequence stars (green curve). The straight blue lines indicate the fitted spectral slopes:  $-1.62$  for the quasar, and  $+3.25$  and  $-0.40$  for the stellar blue and red passbands. Note that these slopes should be multiplied by  $0.4$  if put on the magnitude scale.

trum, and a mean-sequence stellar spectrum (taken from the HILIB stellar flux library, Pickles 1998) in Fig. 3. Since the stars are always observed at zero redshift, and the quasar slope is not depending on source redshift (at least up to  $z \approx 3$  for the blue), redshift effects on the color terms can be ignored. The best fit to the measured values is with a K2 stellar template, but even for a mean field star as blue as G8, or red as K7, we get decent fits, cf. Table 1. A mean stellar type of K2 is reasonable, given the combination of their relative frequency and observed brightnesses of the calibration stars (between  $R = 12$  and  $R = 20$ ), and is consistent with, for instance, the Bahcall & Soneira model for our Galaxy (Bahcall & Soneira 1980, 1981). We do note, however, that the calculated color offsets between the stars and quasars are minimal (though still not zero for  $g_{sdss} - B_{usno-a2}$ ) with a mean F6 spectrum.

Given the predicted color offset values, and the reasonable assumption of a K type dwarf as our mean stellar classification, we feel confident that

the bulk of the offsets are accounted for by this quasar–stellar color offset. There may be other effects at work though, like the Malmquist bias. This bias represents the fact that for a population with a negative number density gradient (i.e., the number of sources increases with decreasing brightness), on average more sources cross a selection limit toward increasing brightness, than the other way around. So variable sources tend to be closer to their peak brightness at their moment of selection (in our case, the SDSS epoch), which in turn means that the color distributions should have slightly negative mean values. Unfortunately, this weak signature is lost in the color offset signal, as it is clear that we have both positive and negative mean offsets in our uncorrected colors. The values listed in Table 1 (and the ones for our adopted mean spectrum of K2) have too many intrinsic uncertainties, like unknown and variable details of the passbands, to be able to determine their values with precision better than  $\sim 0.05$  magnitudes. Therefore, retrieving a magnitude for the Malmquist offset from these particular plots (like Helfand et al. 2001) is not feasible (but see Sect. 4).

It is very important for our structure function analysis (cf. Sect. 3) to have symmetric color distributions with means around zero, so we removed the color offset (including possible Malmquist offsets) by applying the fitted means, and not just the modeled values from Table 1. For the remainder of the Paper these constants should be considered subtracted from each quasar color individually, resulting in the corrected distributions in Fig. 2, right panel.

### 3. Structure Function

Structure Functions (SF hereafter) provide a tool to investigate the time-dependence of variations. It is not very sensitive to aliasing problems due to discrete (and sometimes sparse) time sampling, which makes it well suited to our particular data-set. See Hughes, Aller, & Aller (1992, and references therein) for an introduction to SFs. We define the SF as:

$$S(\tau) = \left( \frac{1}{N(\tau)} \sum_{i < j} [m(i) - m(j)]^2 \right)^{\frac{1}{2}} \quad (1)$$

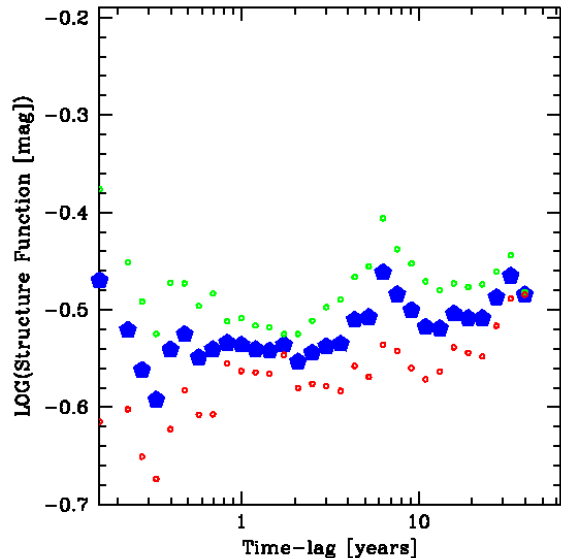


Fig. 4.— Structure Function for our photometric calibration stars. In the absence of systematic increase of measurement uncertainty with age of the observations, the SF should be constant. We detect a slight increase toward longer time-lags, but both the rms level and increase are small compared to our quasar SF. The blue pentagons represent the combined data, and the green and red points above and below the pentagons are the g-band and r-band data separately. Note that the noise levels are lowest in the r-band. The peak in the green data points around a time-lag of 7 years may be due to the relative paucity of data at those time-lags.

analogously to Hawkins (2002). The summation is made over the  $N(\tau)$  measurement pairs for which  $t_i - t_j = \tau$ . In practice one calculates all the possible (positive) time-lag permutations, amounting to  $n(n-1)/2$  difference measurements, with  $n$  being the total number of measurements. After rebinning these into discrete time-lag bins, the SF for each bin is simply given by the rms in the magnitude variations. Since one usually has a large number of difference measurements, a subsequent binning of the bins provides an indication on the error in the SF measurement. This is typically what we have employed in this paper.

### 3.1. Stellar Structure Function

There is some concern our data, since it has been taken at different epochs with different equipment, may have a systematic bias toward higher measurement noise with increasing age of the data. It is quite clear that the most recent SDSS data have by far the best photometric accuracy, and if for one reason or other, the 1950’s era data would happen to have a larger spread in their photometry compared to the GSC2 data, we would have no trouble finding an increase in the rms as a function of epoch. This would slant the SF upward with increasing time-lag, away from the anticipated constant level. Any interpretation based on such a SF would be suspect.

It is therefore that we set out to measure the SF for the calibration stars separately. Again assuming our stars are not variable (on average), their SF should be a constant, reflecting the overall mean magnitude measurement uncertainty. One of the nice side-effects of the quasar redshift distribution is that the time-sampling gets smeared out from its initial measurement lumps around the 1950’s, 1980’s, and 2000, to a more or less uniform sampling by virtue of the  $(1+z)$  time-frame correction. Since our calibration stars are all at  $z = 0$ , no such smoothing out is provided for. We therefore assigned a “redshift” to the individual stars to mimic this effect, randomly selected from the quasar redshift distribution function<sup>3</sup>.

The resulting SF is plotted in Fig. 4, for the combined photometric data and the g- and r-bands separately. The plotting ranges are identical to the other SF plots so it is easy to compare them. While there is a slight increase in SF with increasing time-lag, both the magnitude and slope do not affect our quasar SF to any level of significance (cf. Fig. 8 for example). We feel confident that the trends in the quasar SF reflect real quasar variability behavior.

### 3.2. Structure Function Noise Dependencies

Analyses by Kawaguchi et al. (1998) and Hawkins (2002) rely heavily on the slope of the

<sup>3</sup>We also assigned the calibration stars the redshift of their associated quasar to test for possible hidden systematics. The resulting SF is indistinguishable from the one presented here.

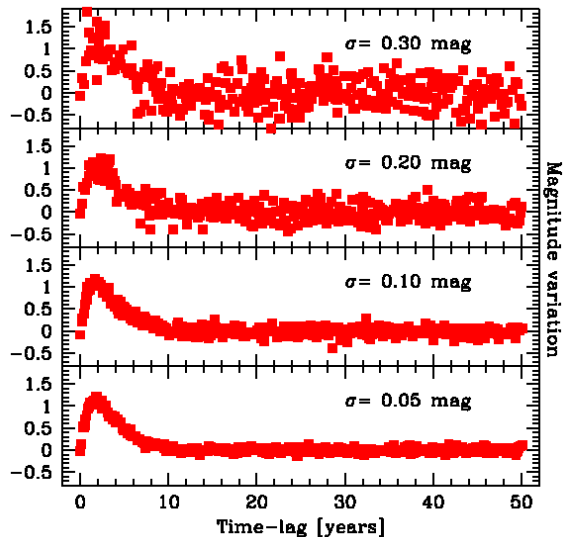


Fig. 5.— Example light-curves with different levels of measurement noise used to generate the structure functions in Fig. 6. The light-curve has the functional form given in Eqn. 2. The Gaussian noise (with indicated  $\sigma$ ’s) has been added to the randomly sampled function.

structure function. In the absence of noise (as noted by Kawaguchi et al.), the slope can be correlated to different light-curves, either due to star-formation, accretion disk instabilities, or microlensing events. Since we know that our data have significant ( $\sigma \approx 0.2$  mag) photometric measurement uncertainties, we need to know the effects of (white) noise on the measurements. For this purpose, we calculated structure functions from a particular light-curve, each with varying degrees of measurement noise (cf. Fig. 5). Aliasing effects due to a fixed time sampling, which would affect the shorter time-lags preferentially, have been minimized by randomly sampling the light-curve. The noise, as added to the analytic form of the light-curve, has a Gaussian distribution with a mean of 0, and the  $\sigma$  as indicated in the plots in Figs. 5 and 6.

The light-curves presented in Fig. 5 are given by the analytical expression (which prescribes both the rise and decay of an outburst, and reaches its peak at  $t = T$ ):

$$L(t, T) = A \left( \frac{e}{T} \right) t e^{-t/T} \quad (2)$$

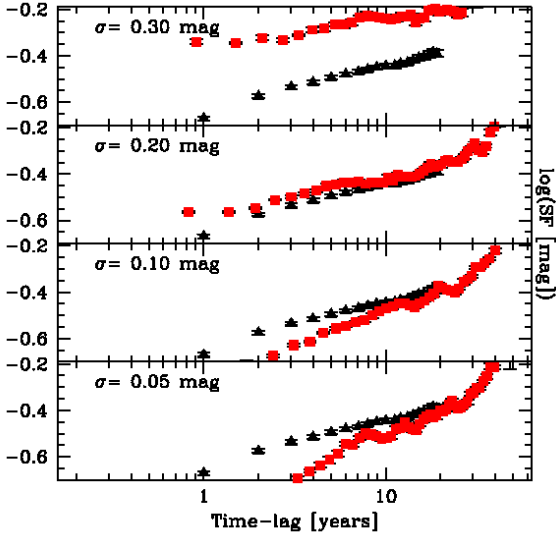


Fig. 6.— Structure functions corresponding to the light-curves in Fig. 5. The largest noise-level dependence is seen for short time-lags, where an increase in noise severely affects the SF level and shape. At larger time-lags, the noise increase tends to smooth out details in the SF, hiding both real and time-sampling / aliasing signals. The overplotted data (small black triangles - Hawkins 2002) would be adequately fitted by a  $\sigma = 0.15$  SF.

with  $t$  in years, and  $L(t, T)$  in magnitudes. The values of  $A$  and  $T$ , which represent the peak variation and brightness decay timescale, have been set to 1.1 (mag) and 1.7 (years) respectively. We chose this particular exponential declining light-curve since it appeared to fit our data particularly well (see Sect. 3.3). Even though our data are actually very sparsely sampled light-curve measurements of individual quasars (on average 3 measurements per band per quasar), the large number of quasars in the sample do allow for an adequate statistical sampling.

Figure 6 depicts the effects of random (Gaussian) photometric measurement noise on the resulting SF. Each light-curve has been quasi randomly sampled in time (with  $0 < \Delta t < 0.3$  years) to minimize aliasing effects in the SF due to a fixed sampling. Our quasar data, once corrected for the source redshifts, exhibits a fairly uniformly spaced light-curve sampling, with on the order of 5 mea-

surements per year over the 50 year base-line. The model light-curve is sampled at a comparable rate of  $\sim 7$  measurements per year. The four panels in the plot have increased noise levels in the light-curves, starting at 0.05 mag in the bottom panel to 0.30 magnitudes in the top panel. A thing to keep in mind is that a *uniform* noise level of 0.05, 0.10, 0.20, and 0.30 magnitudes translates into a *constant* SF with values of  $-1.15$ ,  $-0.85$ ,  $-0.55$ , and  $-0.37$  respectively. It is immediately obvious that this addition of a constant to the SF impacts the curve at short time-lags (where its values are comparable in magnitude) the most: the SF slope decreases significantly, up to the point where it is essentially zero in the top panel. A slightly more subtle effect is also present, in that small (time-scale) structure will get smoothed out.

Given our data quality, both of these effects have to be considered in SF analyses, and obviously limit the extent to which we can push the interpretation.

### 3.2.1. Measurement Noise Levels

We can use the quasar SF, as plotted in Fig. 7, to estimate the intrinsic photometric measurement uncertainties in our data. Since at short time-lags the SF will be dominated by the measurement noise, we can read off the  $\log(S)$  level of this “plateau” directly. This is related to the measurement noise (see, e.g., Hughes et al. 1992) through:

$$\sigma_{\text{noise}} = \frac{1}{\sqrt{2}} 10^{\log(S_p)} \quad [\text{mag}] \quad (3)$$

which for a value of  $\log(S_p) \sim -0.58$  translates into a photometric measurement noise of 0.18 magnitudes. So before any model light-curve can be compared to our data, we have to add 0.18 magnitudes of noise.

## 3.3. Quasar Structure Function

Kawaguchi et al. (1998) correlated various SF slopes to different intrinsic light-curves. For instance, their accretion disk instability model results in typical SF slopes of 0.5, whereas models based on variability due to starburst / supernovae have much steeper slopes ( $\alpha \approx 0.9$ ). The relative robustness of these slopes with respect to other model variables led Hawkins (2002) to compare the SF of a sample of 401 quasars with



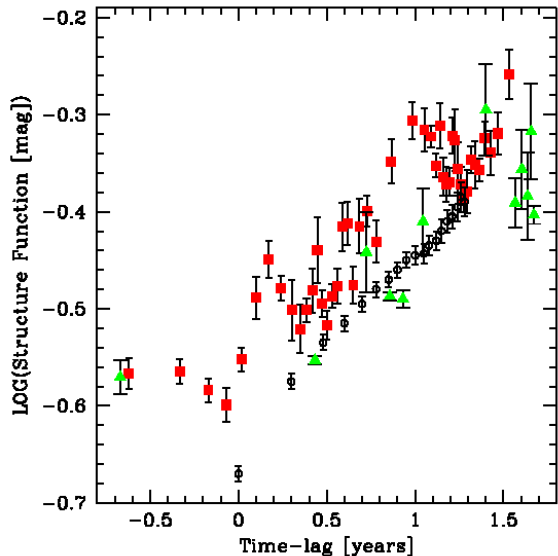


Fig. 7.— Structure function for our quasar sample. Solid, red squares denote time-dilation corrected variations (i.e. source intrinsic), whereas the solid green triangles represent the SF as observed. Overplotted as black circles are data from Hawkins (1996) on a sample of 401 quasars, providing a better photometric quasar baseline. Note the good agreement between the slopes of the data sets. The Hawkins data can be best fitted to our (source intrinsic) SF by offsetting it by 0.08 mag in the y-axis; it is already consistent with the observed SF.

light-curve and redshift information to these predicted model slopes. As another possible variability mechanism, Hawkins suggested (micro)-lensing events, which produce an SF slope  $\alpha = 0.25$  (cf. Table 1 of Hawkins). It is this slope that is consistent with the Hawkins quasar data, suggesting a micro-lensing origin of variability.

In Fig. 7, we present our SF and compare it to the Hawkins data set. Since we have redshift information for all our quasars, we can correct for time-dilation effects. Obviously, if the variations are due to intervening micro lensing events, this correction does not apply. The  $(1+z)$  time-lag correction has the nice side-effect of improving our time baseline sampling. Whereas the non-corrected time-lags are necessarily quantized by the historic observation dates, the corrected ones

get spread out nicely. This accounts for most of the difference between the two SF curves in Fig. 7. The non-corrected data have gaps in their time-lag coverage, resulting in a much less uniform data distribution. The key information from this plot is that both distributions have the same slope, and are consistent with the much better time-sampled Hawkins data set. Effectively, the time-dilation correction shifts the SF over toward shorter time-lags by 0.25 dex along the x-axis. This translates into an inferred redshift of 0.78, which is somewhat less than the median redshift of the sample ( $z_{\text{med}} = 1.46$ ,  $z_{\text{ave}} = 1.49$ ).

Unfortunately, unlike periodic photometric monitoring programs (e.g., the quasar light curve data base of Hawkins 1996) where each quasar is observed multiple times and therefore provides input for each particular time-lag bin (if sampled adequately), our data is much less uniform. We can, however, combine both the g- and r-band datasets to increase the time-sampling a bit, since the POSS and GSC2 surveys in some cases did not take the green and red plates at the same night. Even this only results in about 27 000 magnitude permutations which can be used to construct the SF. So, on average each quasar only adds about 7 data points to the combined light curve. This also implies that the set of quasars contributing to a particular time-lag bin is not constant, which may be partly responsible for the larger spread in the data (cf. Fig. 7) when compared to the Hawkins (2002) data-set.

An added complication is that we do not have any idea about the actual light-curve for each quasar. This does not mean that we cannot infer anything about their shape however. If we assume that to first order all quasar outbursts have comparable shapes (i.e. comparable half-life timescales  $T$ ), and occur on similar characteristic timescales  $P$ , we can use the SF to constrain these parameters. For this purpose we created artificial SFs based on Monte-Carlo simulations of randomly sampled light-curves. Each quasar gets assigned a randomly generated light-curve with multiple outbursts of the form given in Eqn. 2. These outbursts are spaced in time with a characteristic time-scale  $P$ . The probability of an outburst occurring between  $t$  and  $t + dt$  is given by



$$\text{Prob}(t)dt = \left(\frac{1}{P}\right) e^{-t/P} dt \quad (4)$$

(which is identical to the Poisson distribution for the probability that no event occurs in time  $t$ ). This exponential distribution is typical for shot noise models of variability, see e.g., Lochner et al. (1991).

Since our model light-curves are noiseless, we added white noise (with  $\sigma = 0.18$  mag, cf. Sect. 3.2.1) to match the observed noise characteristics. The resulting individual light-curves are more similar to actual light-curves (e.g., Giveon et al. 1999) than the ones presented in Fig. 5 for instance. From these light-curves we then randomly selected 4 measurement points over a  $50/(1+z)$  year time period<sup>4</sup>, resulting in 6 time-lag permutations which are entered into the database. This is done for all 3791 quasars, resulting in an artificial time-lag data-set which is otherwise identical to the actual one, save for the fact that we know it depends on the typical variation amplitude  $A$ , decay time  $T$ , and characteristic outburst time-scale  $P$ .

To get a feel for how particular sets of these randomly sampled light-curves translate into SFs, we note the following: 1) if  $P$  is small (on the order of 50 years or less), the SF shape is determined by the signal due to the typical half-life time  $T$ . But since the outbursts occur fairly regularly, there is a noticeable lack of “variability contrast” at time-scales close to (and beyond)  $P$ : the SF flattens out. 2) the SF at short time-scales is controlled by the half-life time  $T$ . For a given  $T$ , there is basically no real SF signal at time-lags shorter than  $T$ . 3) if  $P$  is large (on the order of a few 100 years), and  $T$  is relatively short ( $< 10$  years) the outburst quickly become “too rare” on the large  $P$  time-scale, and noise starts dominating toward longer time-lags. 4) very short  $T$ ’s ( $\sim 1$  year) are progressively less time resolved given our time-sampling and noise properties. This lessens our ability to make any distinction between their cases.

We can attain acceptable fits to the SF for  $T$  values ranging from 1 to 3 years, and  $P$  values between 100 and 300 years. The “best” values

are  $T \approx 2$ ,  $P \approx 200$  years, and  $A \approx 2.1$ . The value of  $T$  is determined by the presence of signal in the observed SF at time-lags of 1 to 3 years; modeled SFs with larger values of  $T$  do not have enough power at short time-lags to match the observed SF, irrespective of the value of  $P$ . The upper limit on  $P$  is basically set by our noise limits, and therefore a significant increase in sample size will result in a much harder limit. Lower values of  $P$  (at about 50 years) are ruled out since the SF starts to lose power at comparable time-lags; it starts to flatten out beyond what is seen in the data (Fig. 7). It should be noted that a value of  $P \sim 100$  years is of the same magnitude as the sound-crossing time for an accretion disk of a  $10^9 M_{\odot}$  black hole (cf. Courvoisier & Clavel 1991, Trevese & Vagnetti 2002); any variations in the accretion rate would even out across the disk on these time-scales. Also, the  $T \approx 2$  year value is remarkably consistent with time-scales found by e.g., Cid Fernandes et al. (1996 and 2000, 1.5–3.0 years), Cristiani et al. (1996,  $\sim 2.4$  years), Trevese et al. (1994,  $\sim 1$  year), using a variety of data and models. Even though our simulations (and data quality) do not allow for an accurate assessment of  $T$  and  $P$ , it is reassuring that our results are close. It also implies that our initial assumption of the existence of characteristic values for  $T$  and  $P$  for our quasars is valid.

For non-source intrinsic variations (e.g., lensing), fits to the SF tend to be less constrained because of the less uniform sampling of our actual SF. None of the observed time-lags get corrected by their uncorrelated source redshift, and therefore tend to cluster around a few,  $\sim 15$ , and  $\sim 40$  years respectively. Modeling results are comparable to the ones for the intrinsic case, though much less constrained, with a slightly higher likelihood for the combination  $T \approx 3$ ,  $P \approx 400$ , and  $A \approx 2.2$ . This is consistent with the log 0.25 offset between the SF distributions (cf. Fig. 7), which translates into a factor of 1.78 toward longer periods. With a larger data-set it might be possible to discriminate between the intrinsic and external sources of variation based on the SF. This is not possible with the current data-set, however.

Finally, as a consistency check, we can calculate the number of quasars expected to have a variation more than  $5\sigma = 0.90$  magnitudes, given their characteristic light-curve and sample size. This

<sup>4</sup>This is assuming the variations are intrinsic. For external variations (e.g., lensing), one has to use the observed 50 year period.

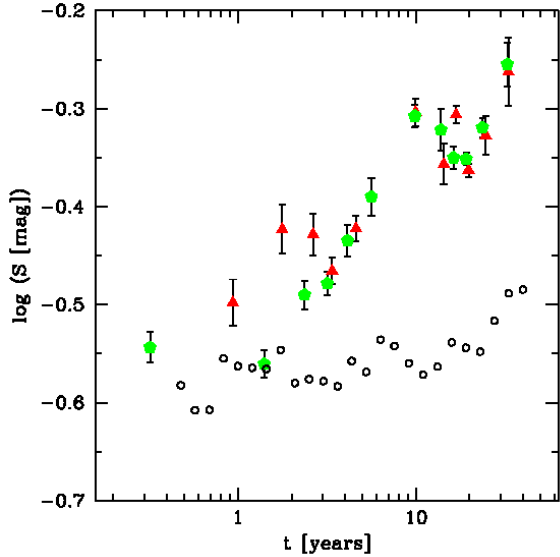


Fig. 8.— Structure function for the quasars. The green pentagons and red triangles represent the SF for the  $g$ - and  $r$ -bands respectively. For time base-lines beyond a few years, the green SF is consistently more variable than the red one. The small black circles represent the SF for the stars in the  $r$ -band, which provides a non-variable base-line.

is done in Sect. 4, but first we will investigate the possible source intrinsic properties that may relate to the SF shape.

### 3.3.1. Color Dependencies

It has been pretty well established that the magnitude of quasar variation is a function of observed (and intrinsic) wavelength. Giveon et al. (1999), for instance, noted a 0.02 magnitude rms difference between B- and R-band variability in a sample of 42 Palomar Green (PG) quasars. The rms in the B–R color variations was found to be 0.05 mag. Variability shifts between the blue and red of this magnitude have been found to be consistent over a range of samples (cf. Trevese & Vagnetti 2002). Wavelength variations in the near-IR tend to be smaller, and are possibly too small to be measured (Enya et al. 2002).

Possible mechanisms for these spectral variations include nuclear star-bursts / supernovae which are predominantly blue (e.g., Aretxaga et al. 1997, Cid Fernandes et al. 2000), and instabilities

in the nuclear accretion disk (e.g., Kawaguchi et al. 1998, Giveon et al. 1999, Trevese et al. 2002). Even variations due to micro-lensing (which are inherently non-intrinsic) could produce a wavelength dependency if there is a *spatial* dependency on wavelength: different parts will be amplified differently, giving rise to the spectral variations. This would occur naturally for accretion disks with a radial temperature gradient.

The two SFs for the  $g$ - and  $r$ -band are presented in Fig. 8. Both SFs have the same slope, but are offset (vertically) by 0.03 in  $\log(S)$ , which is very close to the Giveon et al. (1999) value. This translates into a 7% (or 0.08 mag) larger variation in  $g$  than in  $r$ , again numbers consistent with ones quoted from the literature. The fact that both SFs are consistently offset beyond  $\sim 3$  year time-scales does not reflect any physical color variability dependence (i.e. blue having different time-scales than red), but more underlines the interdependence of the points in SF plots. The slope is a far more robust discriminator (cf. Kawaguchi et al. 1998), and is identical for both bands.

### 3.3.2. Source Intrinsic Dependencies

Our sample contains about 8.5% each of radio-loud and X-ray luminous quasars (322 radio-loud, 328 X-ray luminous, with an overlap of 52 quasars), so we can test whether these are more variable than their radio-quiet and X-ray quiet counterparts. Evidence for this has been found by e.g., Eggers et al. (2000). Furthermore, we can divide the sample up in redshift bins to test for redshift (and consequently luminosity, which is tightly coupled to the redshift) dependencies. Unfortunately, this exercise cannot be carried too far, as pretty quick systematic noise starts to dominate the signal of the small number of quasars per bin.

The median redshift of our sample is  $z = 1.46$ , so we divided our sample up in a low- and high-redshift subset, with the median redshift as discriminator. The resulting SFs are identical to the ones plotted in Fig. 8, and no statistically significant offset is seen. The only difference between the low- and high-redshift SFs is that the latter does not extend toward long time-lags as much as the low-redshift subset. This reflects the intrinsically smaller time-lags for the high redshift bin compared to the low-redshift base-lines (akin to the

offset in Sect. 3.3). Given the correlation between redshift and (absolute) luminosity (cf. Fig. 10), it does not come as a surprise that we do not detect any significant difference between the SFs of faint and bright quasars either. This is further compounded by the fact that brighter quasars (which are on average at higher redshifts) are found to be less variable (e.g., Hook et al. 1994, Trevese et al. 1994), but are also sampled (given our fixed bandpasses) progressively bluer, and more variable. These two (small) effects therefore tend to cancel each other. Improved photometry and a larger sample may help in this respect.

The situation does not improve by isolating just the radio-loud and/or X-ray luminous subsets of our sample. We cannot use the present data-set to separate the radio-loud / X-ray loud SF from their quiet counterpart.

#### 4. Optical Properties of Variable Quasars

From our initial quasar sample of 3791, we selected the 51 sources with a g- and r-band rms in the variability of more than 0.9 magnitude, which corresponds to a variation of more than  $5\sigma$ . These sources are tabulated in Table 2. This number of 51 sources is roughly consistent with the expectation based on a typical light-curve with  $T = 2, P = 200$  years. The length of time this light-curve exhibits more than an 0.9 magnitude variation is about  $\sim 2.5\%$  of the time. This then linearly translates into  $\sim 90$  or so quasars in our sample which would have a variability amplitude of more than  $5\sigma$ .

This most-variable (MV) subsample can be investigated in two ways. First, the MV sources can be compared in its entirety to the main set, and secondly, the MV source set can be intercompared with itself by splitting it up in the ones that are brightest and the ones that are faintest in the SDSS epoch (the epoch with the best photometry).

Based on work by e.g., Trevese & Vagnetti (2002), one expects a color shift during outbursts. Since the quasars in the sub-set which is brighter in the SDSS epoch are presumably undergoing an outburst (in contrast to the fainter set), their colors should be offset from the quasars in the fainter set. Unfortunately, we do not have the non-outburst photometry for each particular quasar in-

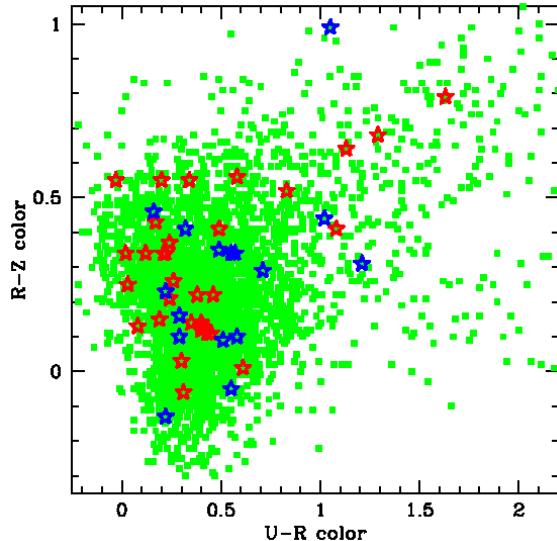


Fig. 9.— SDSS Color-color plot of the most variable quasars (star symbols) compared to the rest of the sample (small green squares). The most variable quasars have been subdivided into ones that are brighter (red stars - 34 objects) and fainter (blue stars - 17 objects) in the SDSS epoch. The disparity in the numbers is due to the Malmquist bias. The small horizontal offset between the two groups may be due to the spectral variability dependency.

dividually (at least not to the required accuracy), so we have to fall back to comparing the statistical properties of the samples. As can be seen in Fig. 9, the quasars span a large range in colors, and simple average quantities will have large uncertainties associated with them. This is further compounded by the very small number of sources in each bin: 34 objects that are brighter in the SDSS epoch, and 17 that are fainter by more than  $5\sigma$ . This apparent disparity between the numbers is due to the Malmquist Bias (as discussed in Sec. 2.1).

We can minimize the impact of outlier points on average values by applying proper weights. In this case we weight the points by their distance from the simple means  $\overline{u-r}$  and  $\overline{r-z}$ . This results in weighted means of:  $\overline{u-r}_B = 0.44$ ,  $\overline{u-r}_F = 0.65$ ,  $\overline{r-z}_B = 0.28$ , and  $\overline{r-z}_F = 0.28$ , where the  $B$  and  $F$  indices indicate whether the sub-set was brighter or fainter at the SDSS epoch. The weighted means for the complete quasar sam-

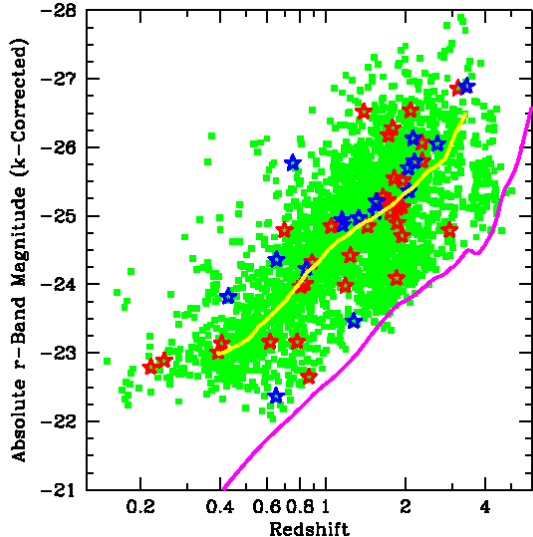


Fig. 10.— Absolute r-Band magnitude of the quasar sample as function of redshift (the “Hubble Diagram”). The most variable quasars are marked by the open star symbols (red for the ones that are brighter, blue for the ones that are fainter in the SDSS epoch). Like in Fig. 9, there is no significant difference between the variable and non-variable populations. All magnitudes have been k-corrected using a quasar composite spectrum. The solid purple line indicates the SDSS r-band detection limit of 20.5 magnitudes. The yellow line represents the median absolute magnitude for the sample (consistent with an observed  $r = 18.7$  median magnitude). Both lines are parallel, indicative of the usefulness of the composite spectrum.

ple are:  $\overline{u - r} = 0.52$  and  $\overline{r - z} = 0.23$ . The color offset between the faint and bright set in  $\overline{u - r}$  (0.21 magnitudes) is probably real, but their absolute value appears to be less certain, given the fact that the overall sample weighted mean falls in between the two. The effects in the  $r - z$  colors are smaller due to the smaller color range and the smaller color variability dependence. A spectral variability dependence, like B to R in the optical (Trevese & Vagnetti 2002) disappears (or becomes too small to measure) in the near infrared (Enya et al. 2002). Given the uncertainty in the average numbers, studies of the spectral dependencies of variability are best done on a small sample of quasars followed through their outburst, instead

of recovering the signal from a large sample of quasars.

Figure 10 illustrates the lack of absolute luminosity dependence on variability. There is no evidence for less luminous sources being more variable (as found by e.g., Hook et al. 1994), at least not based on our data. Cristiani et al. (1996) find no correlation between variability time-scales and absolute luminosity, which would be more consistent with our findings. However, disentangling the correlated effects of sample selection, detection limits, and redshift-luminosity effects have been proven to be notoriously difficult (cf. Giallongo, Trevese, & Vagnetti 1991).

The main result of this section is to show that the (optical) properties of quasars in outburst do not differ from their quiescent phase, at least not in their average sense. The relative fraction of highly variable quasars (both the bright and faint sets) is constant over the range of absolute luminosities. The SDSS photometry should be more than accurate enough to detect small deviations between the two sub-sets, but revealed nothing beyond a small color dependency signal, one that has been measured before (Trevese & Vagnetti 2002).

## 5. Summary

We have demonstrated the applicability of large photometric databases in the long-term variability studies of quasars. The big advantage of this method over detailed monitoring of a smaller set of sources is its scalability. More sources, more catalogs, and more epochs can be added to the existing data-set in a straightforward manner, all of which will improve the robustness of the results.

Our SF analysis of the initial set of 3791 quasars, as retrieved on photographic plates dating from the 1950’s through the 1980’s, combined with the SDSS era CCD photometry, yielded the following results: 1) the variability as function of time-lag is totally consistent with data-set based on close monitoring of quasars, underlining the usefulness of the method; 2) quasars are more variable toward shorter wavelengths, at least beyond time-lags of a few years; 3) their variability is consistent with an exponentially decaying light-curve with a typical half-life time-scale of  $\sim 2$  years; and 4) these outbursts occur on typical time-scales of  $\sim 200$  years.

In a follow-up paper we will discuss the results of a much larger sample of quasars, pending SDSS release of their first data-set.

It is a pleasure to thank Uriel Giveon and the referee, Dr. Trevese, for useful comments that helped improve the paper. WDV's work was performed under the auspices of the U.S. Department of Energy, National Nuclear Security Administration by the University of California, Lawrence Livermore National Laboratory under contract No. W-7405-Eng-48. This research has made use of the NASA/IPAC extragalactic database (NED) which is operated by the Jet Propulsion Laboratory, Caltech, under contract with the National Aeronautics and Space Administration.

## REFERENCES

- Aretxaga, I., Cid Fernandes, R., & Terlevich, R. J. 1997, *MNRAS*, 286, 271
- Bahcall, J. N., & Soneira, R. M. 1980, *ApJS*, 44, 73
- Bahcall, J. N., & Soneira, R. M. 1981, *ApJ*, 246, 122
- Bregman, J. N., Glassgold, A. E., Huggins, P. J., et al. 1990, *ApJ*, 352, 574
- Cid Fernandes, R., Aretxaga, I., & Terlevich, R. 1996, *MNRAS*, 282, 1191
- Cid Fernandes, R., Sodré Jr, L., & Vieira da Silva Jr, L. 2000, *ApJ*, 544, 123
- Courvoisier, T. J.-L., & Clavel, J. 1991, *A&A*, 248, 389
- Cristiani, S., Trentini, S., La Franca, F., Aretxaga, I., Andreani, P., Vio, R., & Gemmo, A. 1996, *A&A*, 306, 395
- Eggers, D., Shaffer, D. B., & Weistrop, D. 2000, *AJ*, 119, 460
- Enya, K., Yoshii, Y., Kobayashi, Y., Minezaki, T., Suganuma, M., Tomita, H., & Peterson, B. A. 2002, *ApJS*, 141, 31
- Fan, J. H., & Lin, R. G., 2000, *ApJ*, 537, 101
- Gal, R. R., de Carvalho, R. R., Odewahn, S. C., Djorgovski, S. G., Mahabal, A., Brunner, R. J., & Lopes, P. 2003, *AJ*, in press (astro-ph/0210298)
- Giallongo, E., Trevese, D., & Vagnetti, F. 1991, *ApJ*, 377, 345
- Giveon, U, Maoz, D., Kaspi, S., Netzer, H., & Smith, P. S. 1999, *MNRAS*, 306, 637
- Hawkins, M. R. S. 1993, *Nature*, 366, 424
- Hawkins, M. R. S. 1996, *MNRAS*, 278, 787
- Hawkins, M. R. S. 2002, *MNRAS*, 329, 76
- Heckman, T. M. 1976, *PASP*, 88, 844
- Helfand, D. J., Stone, R. P. S., Willman, B., White, R. L., Becker, R. H., Price, T., Gregg, M. D., & McMahon, R. G. 2001, *ApJ*, 121, 1872
- Hook, I. M., McMahon, R. G., Boyle, B. J., & Irwin, M. J. 1994, *MNRAS*, 268, 305
- Hughes, P. A., Aller, H. D., & Aller, M. F. 1992, *ApJ*, 396, 469
- Kawaguchi, T., Mineshige, S., Unemara, M., & Turner, E. L. 1998, *ApJ*, 504, 671
- Lochner, J. C., Swank, J. H., & Szymkowiak, A. E. 1991, *ApJ*, 376, 295
- McLean, B. J., Hawkins, G., Spagna, A., Lattanzi, M., Lasker, B. M., Jenkner, H., & White, R. L. 1998, "The Second Guide Star Catalogue", in "New Horizons from Multi-Wavelength Sky Surveys", proceedings of IAU Symposium 179, eds. B. McLean, D. Golombek, J. Hayes, & H. Payne, p. 431
- Monet, D. G., Levine, S. E., Canzian, B., et al. 2003, *AJ*, 125, 984
- Pickles, A. J. 1998, *PASP*, 110, 863
- Rees, M. J. 1984, *ARA&A*, 22, 471
- Reid I. N., Brewer, C., Brucato, R. J., et al. 1991, *PASP*, 103, 661
- Siemiginowska, A., & Elvis, M. 1997, *ApJ*, 482, L9
- Stoughton, C., Lupton, R., et al. 2002, *AJ*, 123, 485

Terlevich, R., Tenorio-Tagle, G., Franco, J., & Melnick, J. 1992, MNRAS, 255, 713

Trevese, D., Kron, R. G., Majewski, S. R., Ber-shady, M. A., & Koo, D. C. 1994, ApJ, 433, 494

Trevese, D., & Vagnetti, F. 2002, ApJ, 564, 624

Vagnetti, F., Trevese, D., & Nesci, R. 2003, ApJ, 2003, June issue



TABLE 1  
DISTRIBUTION COLOR OFFSETS BETWEEN STARS AND QUASARS<sup>1</sup>

Mean Stellar Template	$(g_{sdss} - B_{usno-a2})$	$(r_{sdss} - R_{usno-a2})$	$(g_{sdss} - J_{gsc2})$	$(r_{sdss} - F_{gsc2})$
Measured	+0.38	-0.02	+0.08	-0.10
F6V <sup>a</sup>	+0.10	-0.00	+0.02	-0.00
G0V	+0.15	-0.01	+0.03	-0.02
G8V	+0.24	-0.05	+0.04	-0.06
K0V	+0.24	-0.04	+0.04	-0.08
K2V <sup>b</sup>	+0.34	-0.05	+0.05	-0.09
K7V	+0.54	-0.10	+0.06	-0.21
M1V	+0.54	-0.09	+0.06	-0.23

<sup>1</sup>Units are in magnitudes, and are listed as stellar mean - quasar mean.

<sup>a</sup>Smallest overall color offset.

<sup>b</sup>Best fit to our observed offsets.

TABLE 2  
MOST VARIABLE SUBSET OF QUASARS

RA <sup>a</sup>	DEC	z	r <sub>sdss</sub>	Var <sup>b</sup>	RA <sup>a</sup>	DEC	z	r <sub>sdss</sub>	Var <sup>b</sup>
00 06 54.11	-00 15 33.4	1.727	18.05	+1.09	03 37 06.22	-00 47 47.7	0.751	17.52	-2.30
00 10 22.15	-00 37 01.2	3.156	18.24	+1.00	03 37 37.45	-00 24 57.2	1.186	19.93	+1.02
00 11 30.56	00 55 50.7	2.306	18.50	+1.67	03 44 25.67	00 54 52.8	0.846	19.33	-1.93
00 14 38.28	-01 07 50.2	1.813	18.84	+0.96 <sup>c</sup>	10 22 24.82	00 06 42.5	0.617	19.36	+1.09 <sup>c</sup>
00 16 02.40	-00 12 25.0	2.090	17.90	+1.23	10 23 16.61	00 09 36.3	0.836	18.98	+1.45
00 16 57.00	00 55 32.0	1.754	19.19	+0.94	10 28 36.87	-00 43 14.3	0.219	17.86	+1.08
00 17 35.69	-01 13 25.1	0.805	18.99	+1.17 <sup>c</sup>	10 57 44.32	-00 37 07.0	2.163	18.76	-0.91
00 19 19.31	01 01 52.2	2.312	18.78	+0.95	11 30 12.38	00 33 14.7	1.940	19.68	+1.96
00 20 23.18	-00 11 10.6	1.645	19.01	+1.15	12 04 55.09	00 26 41.3	1.555	18.77	-0.97
00 24 11.66	-00 43 48.1	1.790	17.98	+1.15 <sup>c</sup>	13 06 11.19	-00 09 32.9	0.393	19.19	+1.06
00 27 23.44	-00 16 13.2	1.708	18.92	+1.37	13 07 24.75	00 37 38.5	0.652	18.12	-1.05
00 45 16.00	00 00 42.3	1.548	18.88	-2.33	13 11 08.48	00 31 51.8	0.429	17.93	-1.13
01 21 00.73	-00 15 19.0	0.864	20.35	+0.93 <sup>c,d</sup>	13 22 56.51	-00 59 30.2	1.152	18.46	-2.57
01 41 36.39	-00 10 19.6	0.405	18.48	+1.73	13 38 56.85	00 27 18.3	1.954	18.87	+1.38
01 42 14.74	00 23 24.2	3.405	18.27	-1.09	14 19 51.61	-00 46 05.9	1.940	19.38	+1.10
01 43 55.76	-00 13 38.3	1.156	18.54	-1.21	14 26 50.90	00 51 50.5	1.333	18.72	-0.91
02 00 06.31	-00 37 09.7	2.136	18.33	-1.56	14 46 46.37	-00 31 43.8	0.699	17.90	+0.96
02 21 43.19	-00 18 03.9	2.638	18.74	-1.09	15 13 07.26	-00 05 59.3	1.860	19.55	+0.96
02 31 53.78	-00 32 32.1	1.721	18.97	+0.90	17 00 11.20	60 03 41.6	2.053	18.67	-1.01 <sup>d</sup>
02 34 44.41	00 01 28.7	0.889	18.66	+0.93	17 06 11.40	61 00 52.9	2.061	19.05	-0.98 <sup>d</sup>
02 36 39.59	-00 53 25.5	0.780	19.64	+1.47	17 08 30.25	61 05 17.6	1.050	18.39	+2.57
02 40 52.83	-00 41 11.0	0.246	18.02	+1.12	17 14 42.92	61 11 58.6	0.650	20.11	-1.04
02 47 48.87	-00 01 47.6	1.866	19.32	+0.92	17 16 56.30	55 17 53.0	2.933	20.06	+0.94 <sup>c</sup>
03 10 19.95	01 01 11.5	1.393	17.69	+1.24	17 42 56.09	54 05 28.3	1.439	19.04	+0.96
03 15 42.47	-01 00 51.9	1.238	19.33	+0.95	17 43 55.78	54 00 12.0	1.851	20.29	+0.96
03 37 06.22	-00 47 47.7	0.751	17.52	-2.30	23 49 39.89	-00 13 15.3	1.276	20.15	-0.93 <sup>c</sup>

<sup>a</sup>Units of right ascension are hours, minutes, and seconds, and units of declination are degrees, arcminutes, and arcseconds. Epoch is J2000.

<sup>b</sup>RMS of the optical variability in magnitudes. A '+' ('-') denotes quasars that are brighter (fainter) in the SDSS epoch.

<sup>c</sup>Detected in the radio by FIRST (1.4 GHz).

<sup>d</sup>Detected in X-rays by ROSAT (0.5-2 KeV).